Open access • Report • DOI:10.2172/4793004

Acoustic emission signal analysis in flat plates. — Source link

C.E. Jr. Fitch

Published on: 01 Jan 1969

Topics: Acoustic emission

BNWL-1008
UC-37

10

5-
4-69

[redacted]

ACOUSTIC EMISSION SIGNAL ANALYSIS IN FLAT PLATES

April 1969

[redacted]

AEC RESEARCH & DEVELOPMENT REPORT

BNWL-1008

BATTELLE NORTHWEST
BATTELLE MEMORIAL INSTITUTE PACIFIC NORTHWEST LABORATORY
BATTELLE BOULEVARD, P. O. BOX 999, RICHLAND, WASHINGTON 99352

LEGAL NOTICE

PACIFIC NORTHWEST LABORATORY
RICHLAND, WASHINGTON
operated by
BATTELLE MEMORIAL INSTITUTE
for the
UNITED STATES ATOMIC ENERGY COMMISSION UNDER CONTRACT AT(45-1)-1830

AEC-RL RICHLAND, WASH.

BNWL-1008
UC-37, Instruments

ACOUSTIC EMISSION SIGNAL ANALYSIS IN FLAT PLATES

By

C. E. Fitch, Jr.

Nondestructive Testing Department
Systems and Electronics Division

April 1969

BATTELLE MEMORIAL INSTITUTE
PACIFIC NORTHWEST LABORATORY
RICHLAND, WASHINGTON 99352

Printed in the United States of America
Available from
Clearinghouse for Federal Scientific and Technical Information
National Bureau of Standards, U.S. Department of Commerce
Springfield, Virginia 22151
Price: Printed Copy $3.00; Microfiche $0.65

ACOUSTIC EMISSION SIGNAL ANALYSIS IN FLAT PLATES

C. E. Fitch, Jr.

ABSTRACT

An acoustic emission signal from a deformation or fracture mechanism is assumed to initiate as essentially a point source for detection frequencies in the range of a few megahertz or below. Approximate mathematical expressions for predicting the number of signal reflections and their time separations, and thus total expected signal durations, were derived and studied for flat specimen geometries.

A 1/2-in. thick A-212-B steel plate was used to determine whether experimental observations could be predicted from approximate relationships derived. Both artificial and real acoustic emission sources were tested under a variety of conditions. Observations of good experimental agreement may provide a basis for optimizing signal detection in flat geometries. A preliminary study of pulse shapes and pulse durations was also conducted in experimental attempts to determine source depth as well as range.

CONTENTS

LIST OF FIGURES

LIST OF TABLES

ACOUSTIC EMISSION SIGNAL ANALYSIS IN FLAT PLATES

C. E. Fitch, Jr.

INTRODUCTION

An acoustic emission signal from a deformation or fracture mechanism is assumed to initiate as essentially a point source for detection frequencies in the range of a few megahertz and below. The signals are detected with sensors which, due to their finite size, are simultaneously sensitive to a range of angles. Because of this angular aperture, signals having ray paths other than those on a straight line between source and sensor can be detected. For finite thickness materials, the total signal from an emission event can be a combination of many ray path reflections between boundaries of the sample.

For a point receiver, signals are detected having time delays ranging from a minimum corresponding to the direct rays, to a maximum corresponding to rays which reflect between boundaries an infinite number of times. The signal time length could actually then be infinite if attenuation and spherical wave spreading did not cause the eventual loss of energy. As the frequency is decreased, finite size sensors appear increasingly more like point receivers, and therefore are more susceptible to signal time spreading.

Conversely as the frequency is increased or the sensor size is increased (or both), the angular aperture decreases. For very high frequencies and very large receiver sizes, angle selectivity could be limited to only direct ray paths. This limitation, of course, would reduce the signal duration from one emission event to a minimum value.

The importance, in certain applications, of accurately counting acoustic emission events obviously becomes more difficult when signals overlap in time due to increased duration. Also, in other applications, it is essential to locate the

emission sites as closely as possible. Since signals from successive reflections tend to obscure first arrival information, the location of emission sites by triangulation also becomes more difficult.

From the preceding discussion, it is evident that sensors should be made as large, and detection frequencies as high as possible. However, as the sensor size is increased, practical limits and problems with coupling energy out of the specimens are eventually encountered. Also, as the test frequency is increased, attenuation becomes so great that emission signals do not propagate over substantial distances.

In the following discussion, approximate mathematical relationships were derived which eventually may be used in optimizing the parameters essential to good emission counting and source triangulation in flat specimen geometries.

SUMMARY

Approximate mathematical expressions for predicting the number of signal reflections and their time separation, and thus the total expected signal duration, were derived and studied for flat specimen geometries. Simplifying assumptions were made with regard to the signal ray paths used in the analysis.

Since the angular aperture of a receiver increases with decreasing frequency and size, it was assumed that a frequency as high as possible and a sensor as large as possible should be used. Sensors much larger than 1 in. in dimension were considered impractical. Also, due to attenuation, frequencies much greater than 5 MHz were not considered advisable because of the desirability of sensing emission signals over long distances.

A 1/2 in. thick A-212-B steel plate available for studies was used to determine whether experimental observations could

be predicted employing the approximate relationships derived. Both artificial and real acoustic emission sources were used in a variety of test conditions. Good experimental agreement was observed in all but a few situations and the method may eventually provide a basis for optimizing acoustic emission signal detection in flat geometries. More studies, however, will be necessary before general applicability is ascertained. Curved geometries must also be considered.

In order to obtain useful information about pulse shapes as well as their durations, a preliminary study was conducted. Attempts to synthesize a pulse by calculation and to compare the calculation with the measured result were made. An initially unreflected pulse was measured close to the source and then added to itself a number of times in the proper amplitude and phase proportions so as to simulate a pulse measured at a greater distance. The measured and calculated signals were of comparable shape. Preliminary evidence that sources can be located in depth as well as in range was also provided in these experiments. This technique, of course, has the possibility of determining crack severity by locating its tip depth below the surface.

SIGNAL DURATION

ANALYSIS

In order to study the complex behavior of acoustic emission signals in flat specimens, a simple geometry is needed. In Figure 1a, a plate is shown within which a number of ray paths are constructed. For an emission source located at either edge of the plate, the first few ray paths arriving at a sensor positioned at X are shown. The first arrival ray travels at the 90-degree angle θ_o, and is parallel and adjacent to the plate top surface. The ray emerges or is transmitted into the couplant at an angle θ_o' equal to the critical

angle θ_c'. It is assumed here that the couplant velocity V' is less than the material velocity V. The critical angle is defined in terms of Snell's law as:

$$\frac{\text{Sin } \theta_c'}{\text{Sin } \theta_c} = \frac{\text{Sin } \theta_c'}{1} = \frac{V'}{V} \tag{1}$$

The nth ray emerges as an angle of θ_n' and is also defined in terms of Snell's law as:

$$\frac{\text{Sin } \theta_n'}{\text{Sin } \theta_n} = \frac{V'}{V} \tag{2}$$

The bundle of rays enclosed within the angle θ_c' minus θ_n' is of interest in later discussion.

The emission source can, in fact, be located with equal probability anywhere across the plate thickness. Figure 1b shows the first few ray reflections for a source located at the plate center. It is obvious that the most general picture, which includes all possible rays for all possible source locations, becomes complex and difficult to analyze. However, it can be seen from an inspection of Figure 1 that within the bundle described by θ_c' minus θ_n' (in Figure 1a), the bundle described by θ_o' minus θ_n' (in Figure 1b) is also included. This means that if all possible ray paths orginating at the surfaces of the plate are detected, then signals from all other rays will also be included regardless of the location of the emission source. Therefore, although the results are only approximate, the analysis can be simplified by using only surface sources.

With Figure 1a representing the geometrical situation, the mathematical expressions predicting the number of reflections (n-1), the expected total signal duration, Δt_n, and the spacing between reflections Δt_n minus Δt_{n-1} are sought. These expressions are to be functions of the plate thickness τ, the distance from the source to the sensor X, the velocity of the material

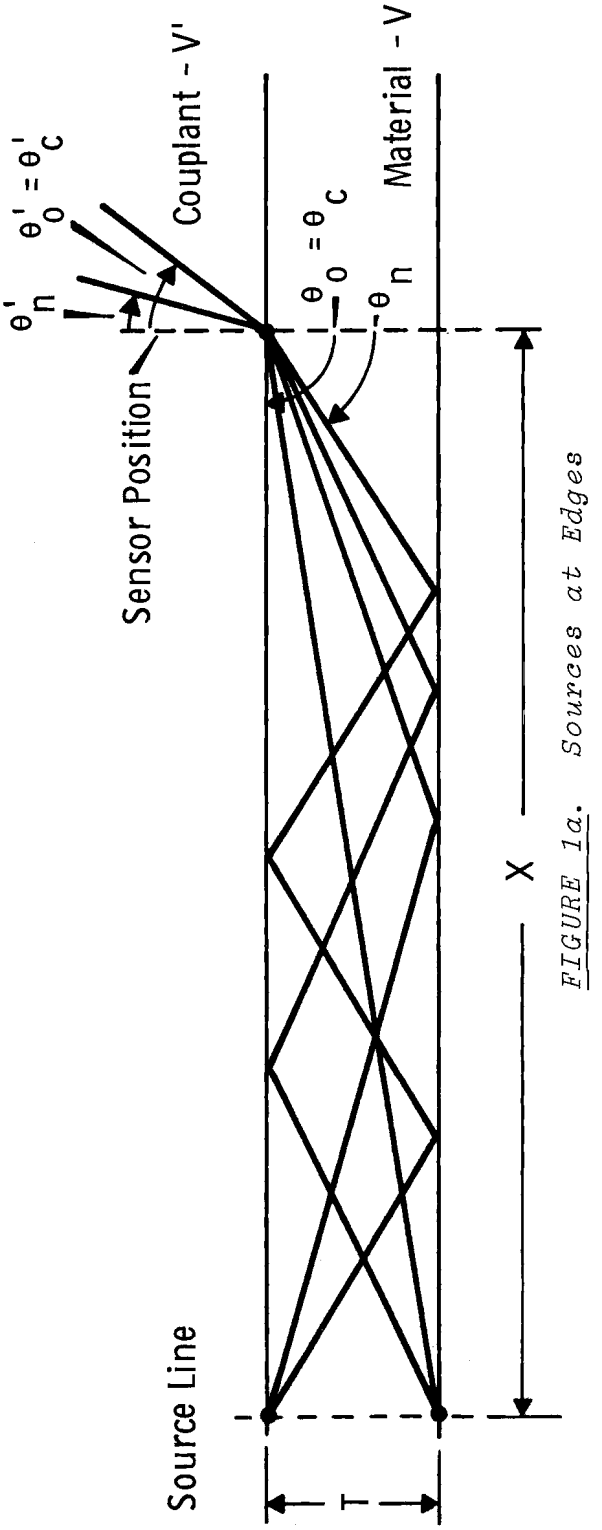

FIGURE 1a. Sources at Edges

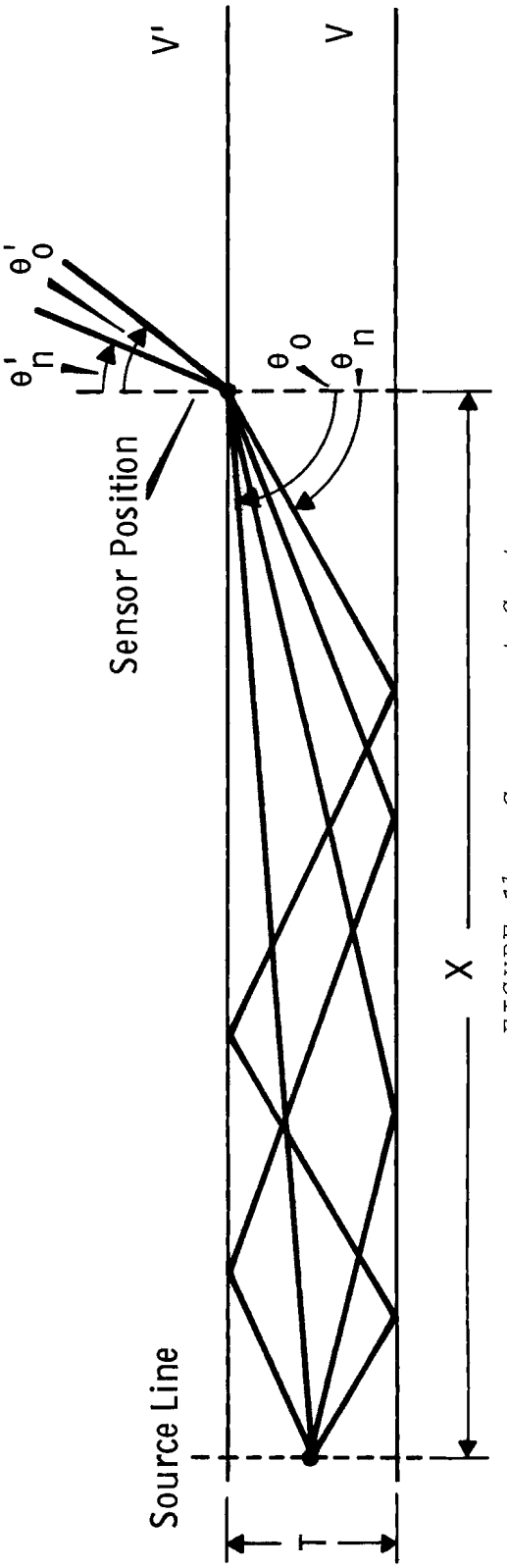

FIGURE 1b. Source at Center

and couplant V and V′, the sensor diameter D, and frequency f. The final objective of the following and subsequent analyses and experiments is then to determine the practical transducer size and frequency and couplant velocity which will minimize the signal duration for a given source location and plate thickness.

Before the analysis proceeds, further discussion about the actual acoustic emission source is desirable. If the material under stress emits acoustic waves as the result of deformation or fracture, it is likely that all types of waves, the longitudinal, shear, and Rayleigh, could be initiated. An ultrasonic transducer had been used in previous preliminary experimental studies as an artificial source of longitudinal acoustic emission waves. Longitudinal waves were introduced at the edge of a plate. It was observed that mode conversion to shear waves produced what was believed to be an intolerable number of signal echoes following the first arrival signal. Since all these echoes emerge into the couplant at the same angle, their elimination by the methods of reducing the angular aperture of the sensor could not be affected. For this reason, shear modes were assumed in the following studies to be the more important of the acoustic emission waves.

Rayleigh waves also require discussion. With an emission source at or near the sample surface, the generation of Rayleigh waves is anticipated. Since the velocity of these waves is near the shear wave velocity, their elimination, again by decreasing the sensor angular aperture, is almost impossible. However, since Rayleigh waves propagate with large surface particle displacements, it is relatively easy to damp them out and yet not appreciably affect the shear waves. Assuming that the Rayleigh waves can be essentially damped out, confining of the analysis to shear waves, as previously mentioned, can also be assumed.

Returning to Figure 1a, the bundle of rays between the angles θ_c' and θ_n' will be designated as:

$$\beta = \theta_c' - \theta_n' \tag{3}$$

It is further assumed that any receiver under consideration will be sufficiently close to the sample to intercept all the rays emitting from the sensor position X shown in Figure 1. Since the sensor has finite size, it will also detect rays emerging at positions other than X. However, since X is almost always large compared with the sensor diameter D, not much error is encountered in assuming all rays to emerge from the point located at X.

The bundle of rays defined by Equation (3) will next be expressed in terms of sensor and couplant parameters. The divergence angle of a sensor is expressed by

$$\text{Sin } \beta \approx \frac{1.22\ V'}{fD} \tag{4}$$

where V' is the couplant velocity, f is the frequency, and D is the diameter (or other controlling dimension if it is not of circular shape). Actually, β is the angle between the normal to the sensor and the outermost ray assumed to be detectable by it. Usually, then, the divergence angle is 2β. However, in the present situation, the normal lies at the critical angle as defined by Equation (1), and rays emerging from the sample theoretically do not exceed this angle. Consequently, Equation (4) adequately represents the bundle of rays described by Equation (3). Solving for D in Equation (4)

$$D = \frac{1.22\ V'}{f\ \text{Sin } \beta} \tag{5}$$

and Sin β must then be expressed in terms of the ray path angles in the sample as shown in Figure 1a. A method thus is provided for limiting β, which limits the detection to a specified number of ray reflections by choosing the correct sensor D and f. From Equation (3)

$$\text{Sin } \beta = \text{Sin } (\theta_c' - \theta_n') = \text{Sin } \theta_c' \text{ Cos } \theta_n' - \text{Cos } \theta_c' \text{ Sin } \theta_n' \quad (6)$$

Also repeating Equation (1)

$$\text{Sin } \theta_c' = \frac{V'}{V} \quad (1)$$

where V is now the shear velocity of the test sample. From Equation (1)

$$\text{Cos } \theta_c' = (1 - \text{Sin}^2 \theta_c')^{1/2} = \left[1 - \left(\frac{V'}{V}\right)^2\right]^{1/2} \quad (7)$$

Inspection of Figure 1a shows that

$$\text{Tan } \theta_n = \frac{X}{n\tau} \quad (8)$$

where n-1 is the number of ray reflections permissible by β in Equation (4). From (8)

$$\text{Sin } \theta_n = \frac{X}{(n^2\tau^2 + X^2)^{1/2}} \quad (9)$$

and from Equation (2) and Equation (9)

$$\text{Sin } \theta_n' = \left(\frac{V'}{V}\right) \frac{X}{(n^2\tau^2 + X^2)^{1/2}} \quad (10)$$

and then

$$\text{Cos } \theta_n' = \left[1 - \left(\frac{V'}{V}\right)^2 \frac{X^2}{n^2\tau^2 + X^2}\right]^{1/2} \quad (11)$$

Then putting Equations (1), (7), (10), and (11) into (6) and, subsequently, Equation (6) into (5),

$$D = \frac{1.22\, V^2\, (n^2\tau^2 + X^2)^{1/2}}{f\left\{\left[V^2(n^2\tau^2 + X^2) - (V')^2X^2\right]^{1/2} - \left[V^2X^2 - (V')^2X^2\right]^{1/2}\right\}} \quad (12)$$

Equation (12) can, therefore, be used to calculate the sensor diameter D needed to limit the received signal to a prescribed number of reflections (n-1) for a given f, V, V', τ, and X.

It is usually handier to assume that a certain diameter and frequency sensor is available. It is better, therefore, to solve Equation (12) for n which then calculates the total number of reflections expected for a given experimental situation. Solving Equation (12) for n yields

$$n = \frac{X}{\tau}\left\{\frac{2\ell^2 m^2}{(1-\ell^2)^2} - 1 + \frac{1}{1-\ell^2}\left[1-2\ell m+4\ell m\left(1 - \frac{2\ell m+\ell^2}{1-\ell^2} + \frac{4\ell^2 m^2}{(1-\ell^2)^2}\right)^{1/2}\right]\right\}^{1/2} \quad (13)$$

where

$$\ell = \frac{1.22\ V}{fD} \quad (14)$$

and

$$m = \left[1 - \left(\frac{V'}{V}\right)^2\right]^{1/2} \quad (15)$$

Equation (13) thus calculates the number of expected reflections for the given test conditions.

It is also useful to determine the expected signal duration for any number of reflections. Referring back to Figure 1a, the first arrival ray travels the distance X in an amount of time

$$t_o = \frac{X}{V} \quad (16)$$

The nth ray arrives at a time

$$t_n = \frac{1}{V}\left(X^2 + n^2\tau^2\right)^{1/2} \quad (17)$$

and the time difference is

$$\Delta t = t_n - t_o = \frac{\left(X^2+n^2\tau^2\right)^{1/2} - X}{V} \quad (18)$$

By calculating n from Equation (13), and inserting its value into Equation (18), the approximate received signal duration for a single acoustic emission event is obtained. By choosing different n values, Equation (18) can also be used to determine the time duration between successive reflections.

Another useful form of Equation (13), obtained by assuming that $V = V'$, expresses the situation, for instance, where the sensor is coupled directly to the edge of a plate, recessed in a hole, or in some other way aligned to receive energy at an emergency angle θ_c', approximately equal to 90 degrees. When

$$V = V'$$

$$n = \frac{X}{\tau}\left(\frac{\ell^2}{1-\ell^2}\right)^{1/2} \tag{19}$$

This is a desirable test condition, since it can be shown for a given D, f, X, and τ that n is a smaller number when $V' = V$ than when $V' < V$.

EXPERIMENTS

Experimental studies were undertaken to determine how well the previously derived expressions predict actual observed results. A source of real acoustic emission signals as well as a sample suitable for using artifical signal sources was considered desirable. An artifical signal source was regarded useful for checking the analytical results and for eventual comparison with the actual emission signal behavior.

A 1/2 in. thick A-212-B steel plate having an area of about 2 ft by 3 ft was available. A "V" groove was cut across the 2-ft dimension about 6 in. from one end of the plate. This 6-in. section was then cut with a band saw into about 1/2-in. strips paralleling the 3-ft dimension and extending from the end to just beyond the "V" groove. It was then planned that the bending of these strips to eventual failure would provide a good source of multiple acoustic emission signals.

Prior to the emission signal studies, artifical sources were studied. A small ultrasonic shear wave transducer was mounted on the end of the plate opposite to where the strips had been cut. A section of this edge had been machined flat

and smooth for good transducer coupling. The pulsing of this small transducer with a short, repetitive burst signal transmitted shear waves into the plate.

As mentioned earlier, use of the highest possible frequency for detecting acoustic emission signals is desirable for good counting and triangulation. Most industrial steels and stainless steels have high shear wave attenuation due to grain scattering for frequencies of 5 MHz and above. Since it is also desirable to be able to detect emission signals as far from the source as possible, the detection frequencies should not be too high. At the present time, only limited attenuation data are available for A-212-B steel. It is anticipated, however, that, for frequencies in the range of a few megahertz, only a few dB/ft of signal attenuation will occur. The major loss mechanism, of course, is due to the inverse distance loss by the spreading out of waves from a point source.

Frequencies of 2 MHz and 4.5 MHz were, therefore, chosen for studies since sensors were also available. The expected number of reflections and signal durations were calculated for these frequencies, assuming transducers were located at X distances from the source of 5, 15, and 30 inches. It was convenient, in most of the experiments, to use water to couple energy out of the plate into the sensors. For water $V' = 0.587 \times 10^5$ in./sec and for A-212-B steel $V = 1.28 \times 10^5$ in./sec. The transducer diameters available for frequencies of 2 MHz and 4.5 MHz were 0.215 and 0.75 in., and 0.1875 and 0.75 in, respectively. Table 1 shows the number of reflections n-1, with n determined by Equation (13), and the expected signal durations Δt, as determined by Equation (18). Also as an aid to determining the total signal duration (Δt) from the total number of reflections (n-1), a graph was prepared in Figure 2 to show the three X positions.

TABLE 1. Signal Reflections and Durations

$V = 1.28 \times 10^5$ in./sec
$V' = 0.587 \times 10^5$ in./sec
$\tau = 0.5$ in.

f, MHz	D, in.	X, in.	n - 1	Δt, μsec
2	0.215	5	8.4	14.4
2	0.215	15	27.3	44.5
2	0.215	30	55.6	88
2	0.75	5	3.3	3.5
2	0.75	15	11.9	10.5
2	0.75	30	24.7	21
4.5	0.1875	5	4.8	6
4.5	0.1875	15	16.5	18.5
4.5	0.1875	30	33.9	36.5
4.5	0.75	5	1.9	1.6
4.5	0.75	15	7.6	4.8
4.5	0.75	30	16.1	9.4
$V = V' = 1.28 \times 10^5$ in./sec				
2	0.1875	30	26.4	23.5
4.5	0.1875	30	10.3	4

This graph can also be used to determine the time between successive reflections (e.g., Δt for the second reflection minus Δt for the first, etc.)

The measured pulse lengths using the artificial source of shear waves corresponding to those calculated in Table 1 are shown in Figures 3 and 4. As mentioned previously, the small shear transmitting transducer was mounted at the plate edge and the receiving sensors were placed at the various X locations. The calculated Δt values are seen to be approximately representative of the measured signals.

An important aspect of the measured signals has not yet been discussed. The shear waves were mode converted to

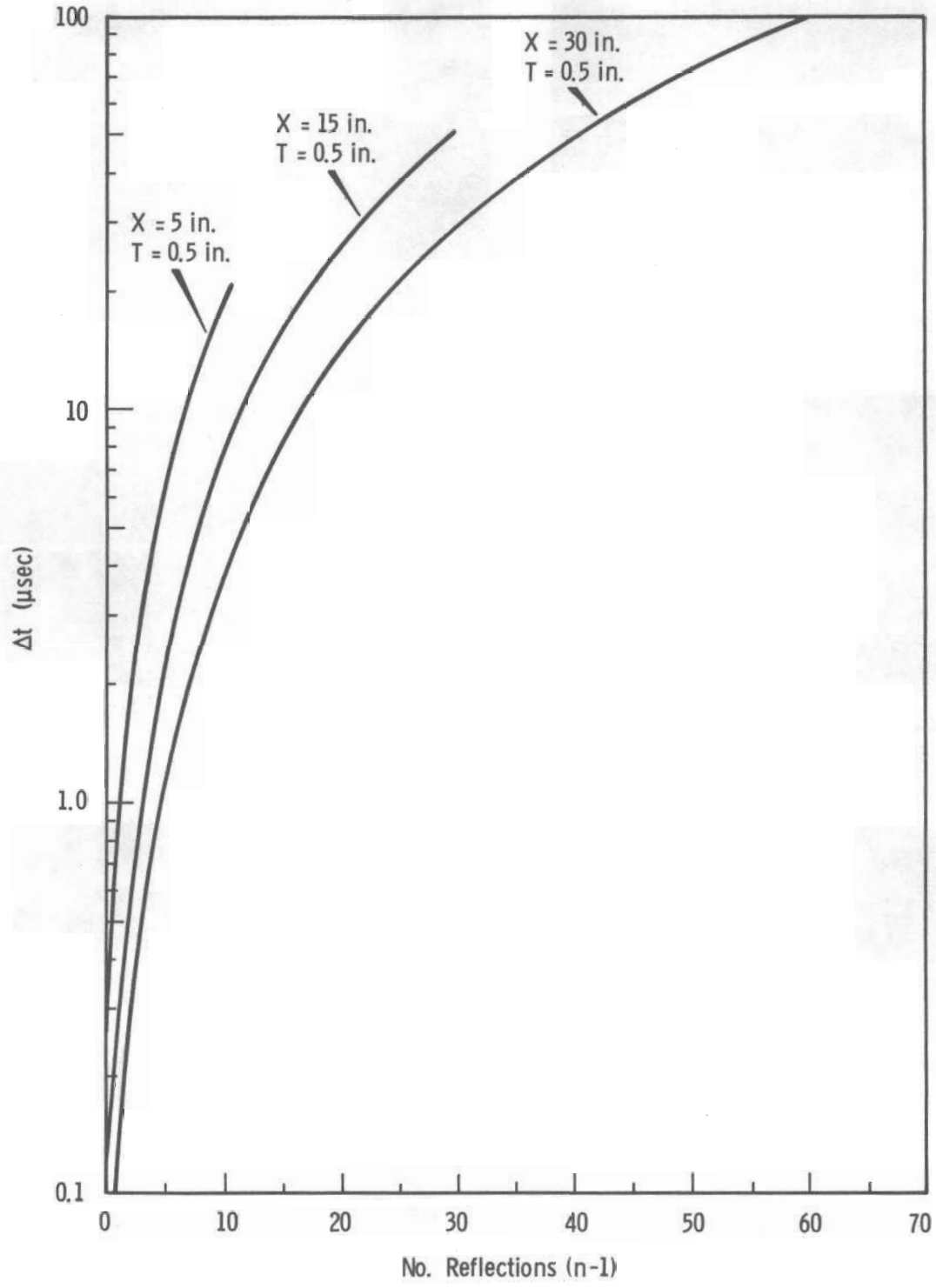

FIGURE 2. Number of Reflections Versus Time Duration

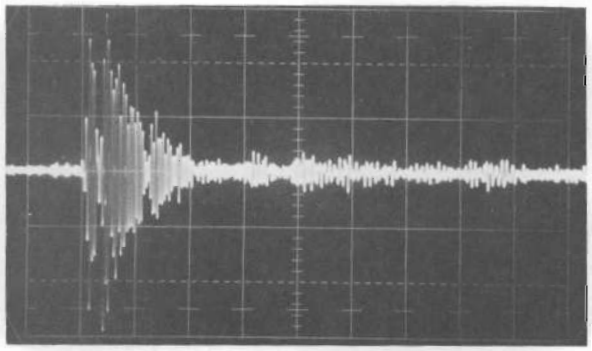

D = 0.215 inches, X = 5 inches
Calc. Δt = 14.4 μsec
Time Scale = 10 μsec/cm

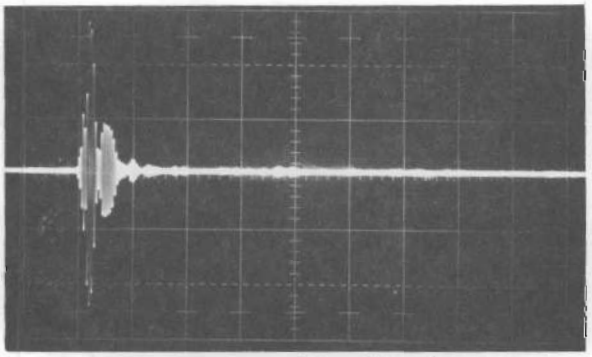

D = 0.75 inches, X = 5 inches
Calc. Δt = 3.5 μsec
Time Scale = 10 μsec/cm

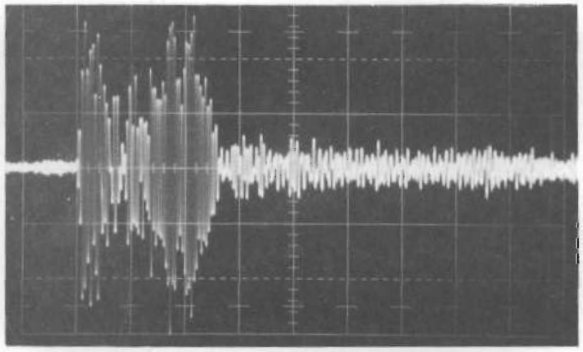

D = 0.215 inches, X = 15 inches
Calc. Δt = 44.5 μsec
Time Scale = 10 μsec/cm

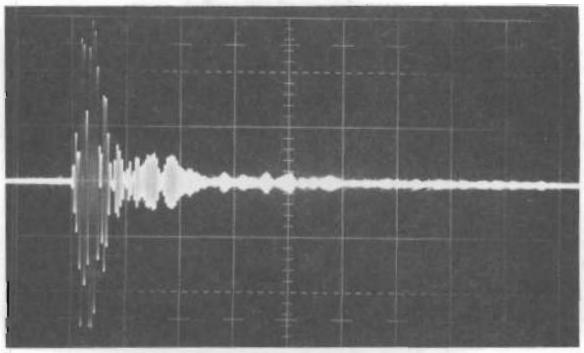

D = 0.75 inches, X = 15 inches
Calc. Δt = 10.5 μsec
Time Scale = 10 μsec/cm

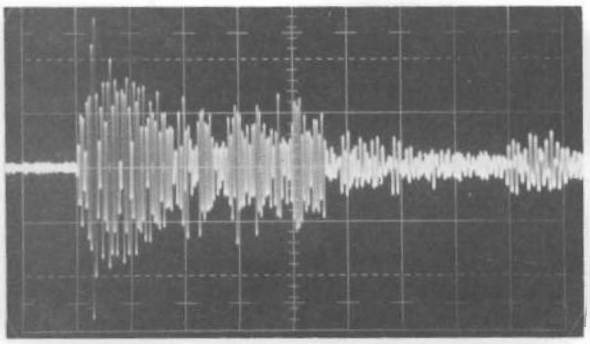

D = 0.215 inches, X = 30 inches
Calc. Δt = 88 μsec
Time Scale = 10 μsec/cm

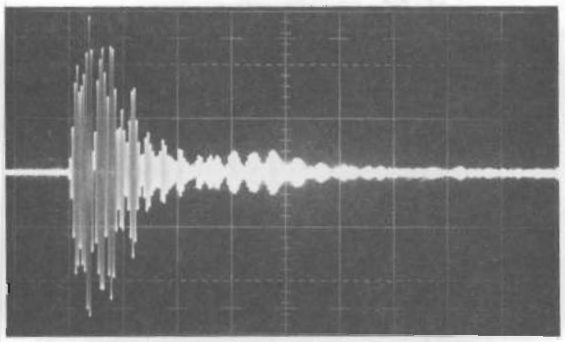

D = 0.75 inches, X = 30 inches
Calc. Δt = 21 μsec
Time Scale = 10 μsec/cm

FIGURE 3. Measured Signals for Artificial Source at Frequency of 2 MHz

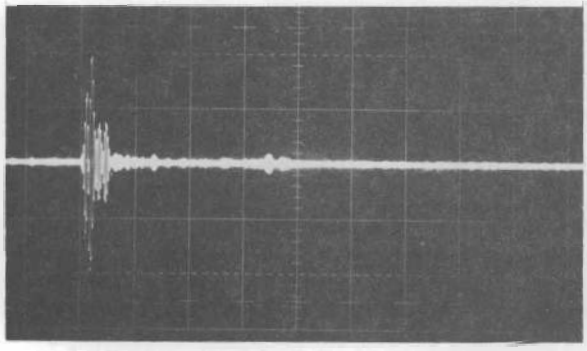

D = 0.1875 inches, X = 5 inches
Calc. Δt = 6 μsec
Time Scale = 10 μsec/cm

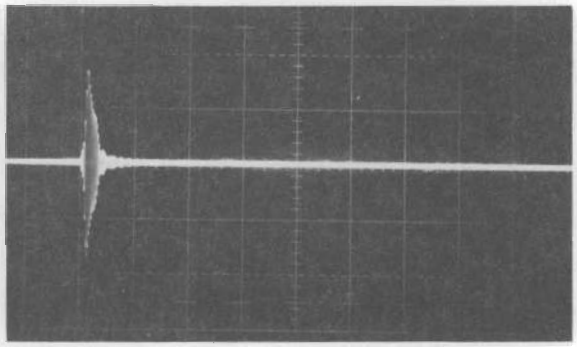

D = 0.75 inches, X = 5 inches
Calc. Δt = 1.6 μsec
Time Scale = 10 μsec/cm

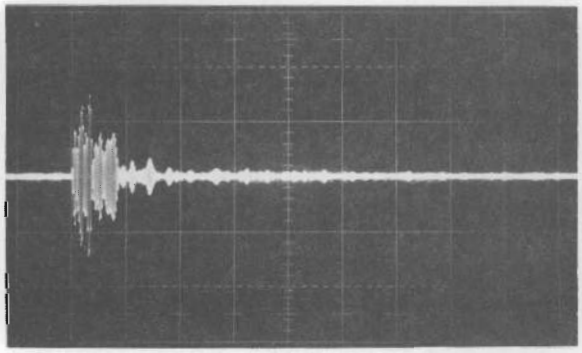

D = 0.1875 inches, X = 15 inches
Calc. Δt = 18.5 μsec
Time Scale = 10 μsec/cm

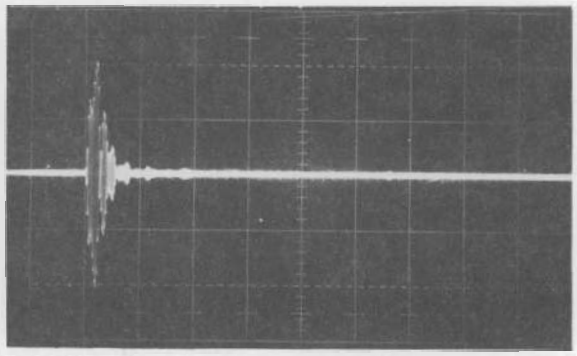

D = 0.75 inches, X = 15 inches
Calc. Δt = 4.8 μsec
Time Scale = 10 μsec/cm

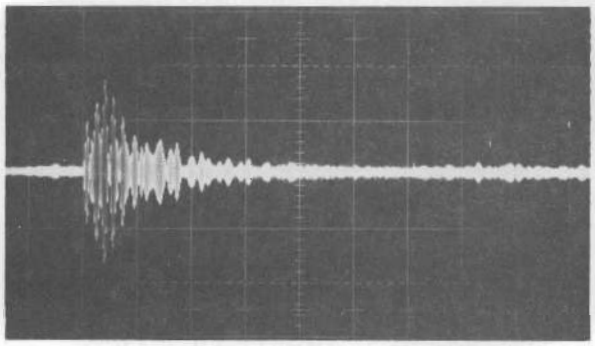

D = 0.1875 inches, X = 30 inches
Calc. Δt = 36.5 μsec
Time Scale = 10 μsec/cm

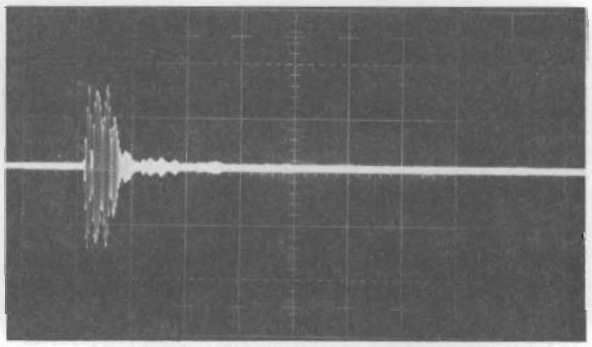

D = 0.75 inches, X = 30 inches
Calc. Δt = 9.4 μsec
Time Scale = 10 μsec/cm

FIGURE 4. Measured Signals for Artificial Source at Frequency of 4.5 MHz

longitudinal waves and received through a water couplant between the sample and sensor. Thus, longitudinal receivers were used. The transmission factor between a solid (metal) and a liquid (water) for shear waves converting to longitudinal waves varies as a function of shear wave incident angle. A small bundle of shear wave rays propagating down the plate approximately parallel to its surfaces without appreciable reflection at the surfaces has a low transmission factor. The transmission factor is higher for a similar bundle propagating at a slightly oblique angle with respect to the surfaces. The first arriving unreflected signals are, therefore, of smaller amplitude than subsequent signals from obliquely traveling rays reflected between the surfaces. The signal thus starts at a low amplitude and builds up with time until subsequent reflections at refraction angles eventually exceeding β in Equation (4) finally initiate decay. These rise and decay effects are illustrated in Figures 3 and 4.

In Figures 5 and 6, measured signals are shown for actual acoustic emission sources. The sensors were positioned at the various locations corresponding to those in Figures 3 and 4. The sensors were always placed in a straight line extending from the particular single edge notch tab being bent. A separate shear wave critical angle sensor was placed as near as possible to the notch to supply a signal for triggering the display oscilloscope. Because each acoustic emission event is expected to be unique, comparison of signals at various distances required the simultaneous observation of the same signal at two locations. This comparison was accomplished with a dual beam oscilloscope, and the traces shown in Figures 5 and 6 were adjusted with independent time delays to present the signals simultaneously.

In comparing the signals in Figures 5 and 6 with those of Figures 3 and 4, the actual acoustic emission signals appear

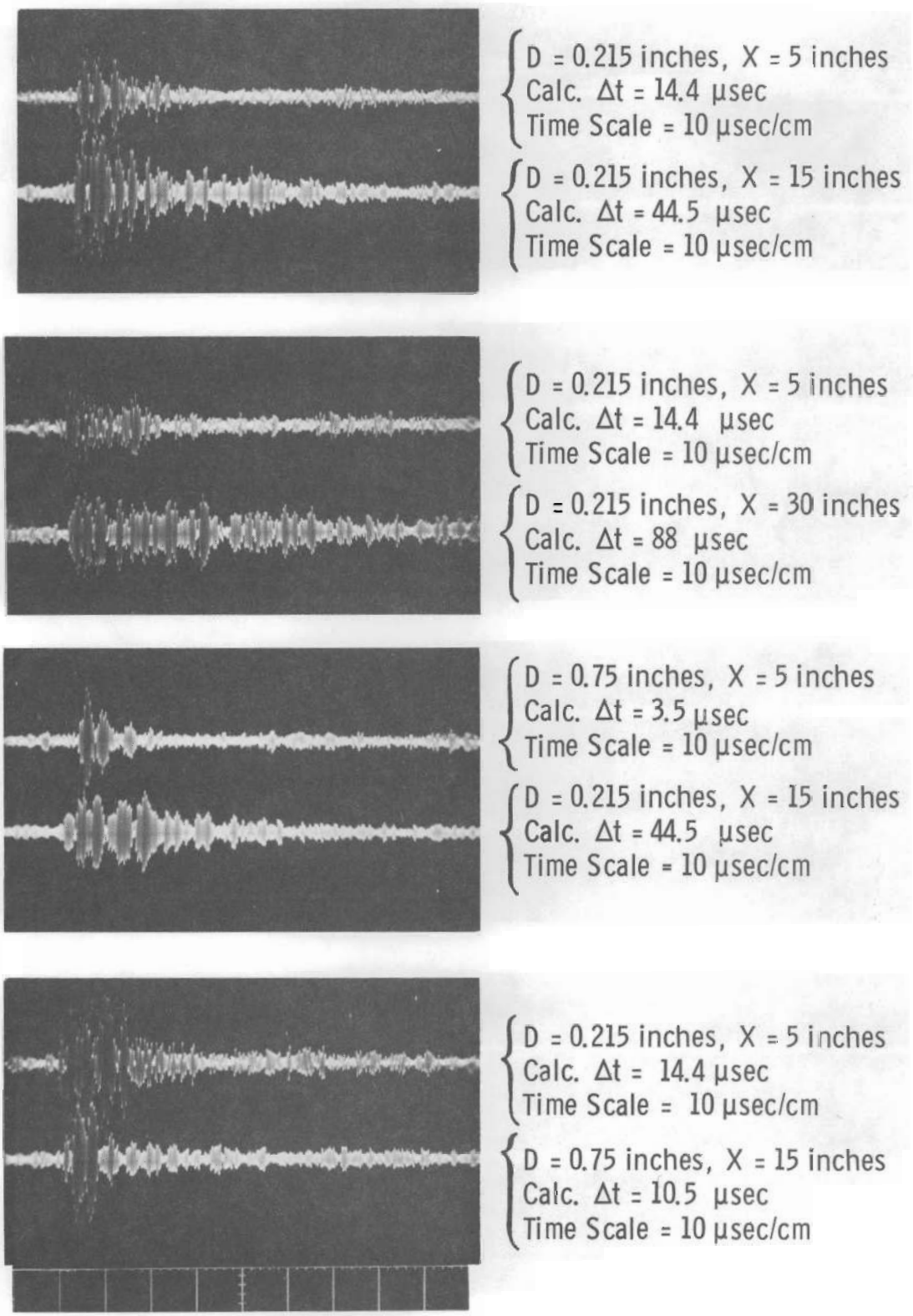

FIGURE 5. Measured Signals for Actual Emission Source at Frequency of 2 MHz

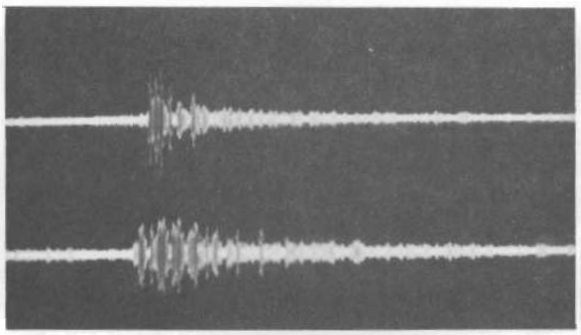

D = 0.1875 inches, X = 5 inches
Calc. Δt = 6 μsec
Time Scale = 10 μsec/cm

D = 0.1875 inches, X = 15 inches
Calc. Δt = 18.5 μsec
Time Scale = 10 μsec/cm

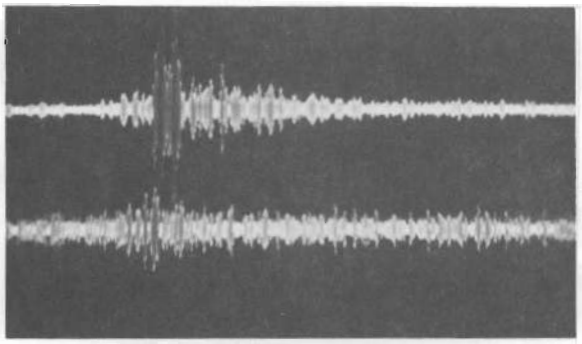

D = 0.1875 inches, X = 5 inches
Calc. Δt = 6 μsec
Time Scale = 10 μsec/cm

D = 0.1875 inches, X = 30 inches
Calc. Δt = 36.5 μsec
Time Scale = 10 μsec/cm

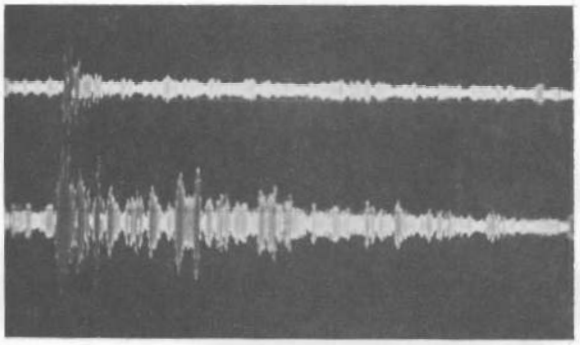

D = 0.75 inches, X = 5 inches
Calc. Δt = 1.6 μsec
Time Scale = 10 μsec/cm

D = 0.1875 inches, X = 15 inches
Calc. Δt = 18.5 μsec
Time Scale = 10 μsec

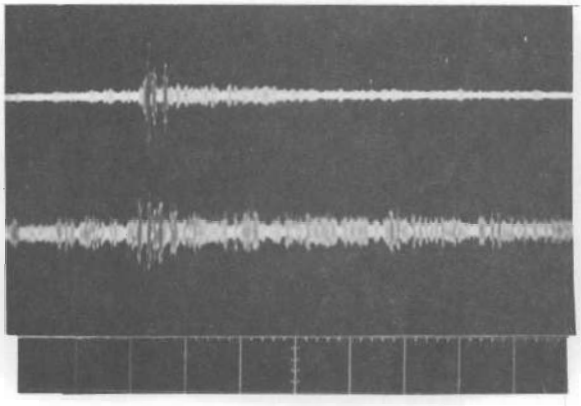

D = 0.1875 inches, X = 5 inches
Calc. Δt = 6 μsec
Time Scale = 10 μsec/cm

D = 0.75 inches, X = 15 inches
Calc. Δt = 4.8 μsec
Time Scale = 10 μsec/cm

FIGURE 6. Measured Signals for Actual Emission Source at Frequency of 4.5 MHz

to also be approximately represented by the previously derived expressions. Differences, however, should be expected between signals from artificial as opposed to real emission sources because an emission burst can occur randomly at any time or position (near the notch), whereas the artificial source has periodicity and a fixed position.

In some instances, emission signals are not shown in Figures 5 and 6 for the 30-in. critical angle sensor positions for the reason that the emission signals were not visible most of the time above the noise at the 30-in. position. Those few that were larger in amplitude were only barely perceptible above the noise. This result is not surprising since the acoustic emissions are essentially from point sources. The major loss in energy then is due to the spreading out of the spherical waves. Since the sensors are pressure sensitive, the loss of signal amplitude varies inversely with distance from the source. For instance, a sensor placed at 30 in. would show only 1/100th the amplitude measured at 0.3 in. Additional losses occur due to attenuation, and amplitude losses in the first arrival wave fronts occur due to the transmission factor variations mentioned previously.

All of these effects makes it difficult to detect acoustic emission signals at distances much beyond a few feet from the source. The amplitude of the signal can be increased somewhat by an increase in angular aperture (β) due to the increase in the net transmission factor. However, as has been shown in the preceding examples, the time increase in signals may make difficult the accurate location of sources by triangulation methods. Accurate measures of crack propagation rate, as determined by signal count rate, may also be difficult. Higher detection sensitivity would make triangulation and counting easier in most applications.

One notable improvement in sensitivity was achieved by using shear wave sensors in place of the critical angle sensors. About an order of magnitude increase in signal was observed by mounting the shear sensors on the edge of the 1/2-in. plate. The signal also decreased in time duration because of the smaller angular aperture as calculated by Equation (4). An example of the signal for an edge-mounted 2 MHz shear sensor having about 1/2-in. dimensions is shown in Figure 7. In Table 1, Δt was also calculated for X = 30 in. and V = V′, and the result was compared to the observed signal in Figure 7. The corresponding signal at X = 30 in. for about the same size (D = 0.215 in.) critical angle sensor is also shown.

The question arises as to how such shear sensors can be mounted in practice if the additional sensitivity is desirable. Since the sensors can be dimensionally quite small, a shallow hole or indentation enabling the sensor to be recessed may be permissible. Also, the geometry of the test sample may provide natural corners for attaching shear sensors in desirable locations and orientations. Other ways of increasing sensitivity may also be possible.

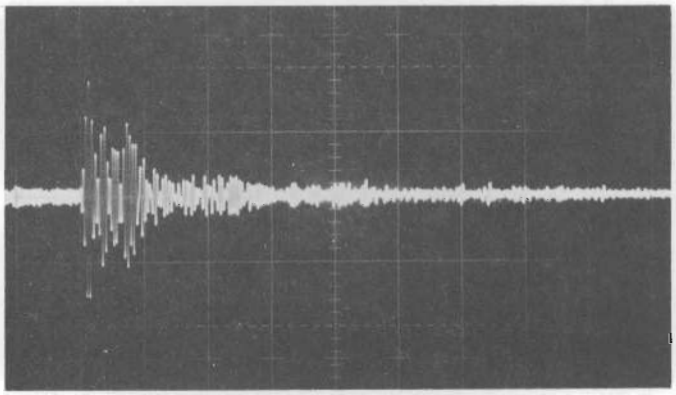

Edge Mounted Shear Sensor
D = 0.1875 inches, X = 30 inches
Calc. Δt = 23.5 µsec
Time Scale = 10 µsec/cm

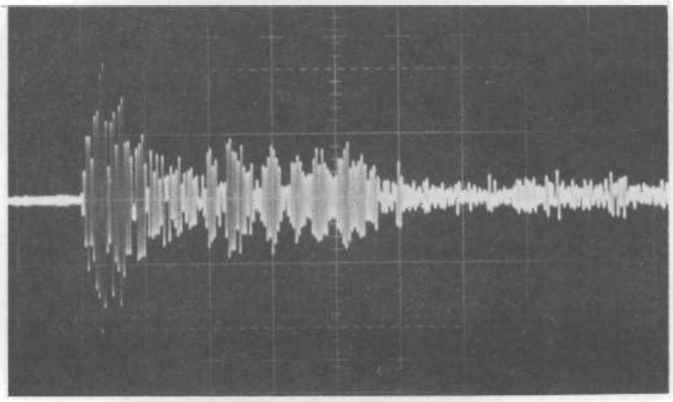

Critical Angle Sensor
D = 0.215 inches, X = 30 inches
Calc. Δt = 88 µsec
Time Scale = 10 µsec/cm

FIGURE 7. Edge Mounted Shear Versus Critical Angle Sensor

SIGNAL PULSE SHAPE

In analyzing acoustic emission wave behavior, the signal pulse shapes as well as their durations must be determined. Knowledge of pulse shapes as a function of sample thickness, receiver distance from the source, etc., are important for obtaining source location by triangulation and for properly devising counting systems capable of determining crack growth. When the previously discussed pulse duration studies were undertaken, information about reflection factor amplitude and phase and the shear wave attenuation coefficients for A-212-B were not known. The partial determination of these quantities has made possible the preliminary study of pulse shapes.

In order to determine actual signal pulse shapes from acoustic emission events, knowledge of the failure mechanism would be necessary in describing the initial disturbance. Then, since a wide band of frequencies will be likely in the initial disturbance, attenuation coefficients must be known over the range of frequencies in the pulse. This knowledge would be necessary in determining pulse shape changes due to excessive high frequency scattering which removes higher frequencies from the pulse in greater amounts than the lower frequencies. It would be necessary, finally, to have accurate knowledge of receiving transducer transfer functions and other acousto-electrical quantities to obtain the eventual pulse shape estimates. These quantities are not entirely available at the present time and some would be difficult to obtain.

Another approach requiring only a limited knowledge of these effects is available. In most practical applications, the propagation of acoustic emission signals over substantial distances, as mentioned previously is desirable. Many of the higher frequency components in the initial disturbance are quickly removed in a short path length due to scattering. For example, the attenuation coefficient in Figure 8 is plotted as

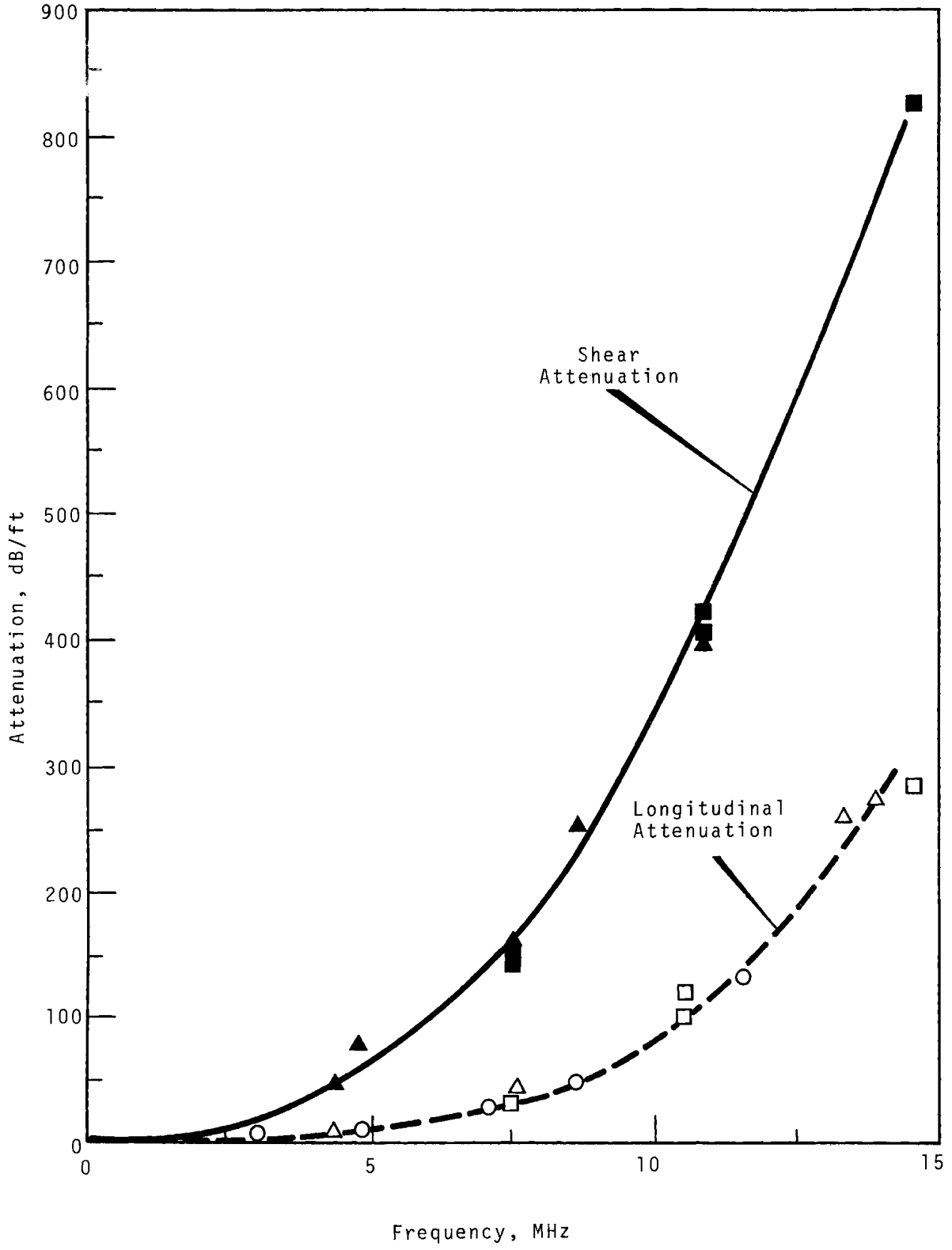

FIGURE 8. Plot of Attenuation Versus Frequency in 304L SS

a function of frequency for shear waves in small grain 304L stainless steel. Scattering losses increase beyond the knee in the curve in approximate proportion to the fourth power of frequency. It is evident then that frequencies beyond a few MHz do not propagate more than a few inches before they are much smaller in amplitude than the lower frequencies.

Although the curve shown in Figure 8 applies to 304L stainless steel, a similar situation is expected in the small grain A-212-B carbon steel used for the present studies. Therefore, emission events initially having a wide frequency band become filtered so that their dominant frequencies are essentially less than a few MHz after traveling a few inches. Signal frequencies below 1 MHz can often be assumed undesirable in practical applications because of hydraulic noises, etc. These lower frequencies, moreover, have the effect of excessively increasing received signal durations. For these reasons, it appears that relatively narrow band receivers with center frequencies of 1 to 2 MHz should be used in field tests. Actual optimum band widths, although apparently in the range of 0.5 to 0.75 MHz, should be determined.

It was therefore decided in the pulse shape studies to use a narrow frequency band width less than 1.5 MHz so that only the attenuation at the center frequency is 1.5 MHz. The attenuation factor for shear waves in A-212-B at this frequency was measured to be about 1.3 dB/ft. Also because of the narrow band width and this low attenuation, no appreciable pulse distortion due to the aforementioned scattering effect was effected.

As mentioned previously, the initial emission pulse shapes within the A-212-B plate and transducer transfer functions should be determined. However, it was assumed in testing the feasibility of signal synthesis methods that the signals could be measured near to the emission site so that no

interference from reflections within the plate could occur. Then, by using the same receiver and electronic system, the signal could be measured again at a greater distance from the source to include the effects of many reflections. The number of reflections, their reflection factor amplitudes and phases, and their differences in attenuation (because of different path lengths) and the pulse shape at the closer distance are known. It was thought possible, therefore, to predict the pulse shapes at greater distances.

This method of determining pulse shapes does not require actual acoustic disturbances within the plate or transducer transfer functions to be known. Provided that the emission signals for a particular test application can be measured before reflections occur, and assuming the test sample geometry is known, it should then be possible to predict pulse shapes in most of the field test applications encountered in practice.

Preliminary pulse shape synthesis experiments were conducted on the 1/2-in. thick A-212-B carbon steel plate used in previous studies. A small point source shear wave transducer was used as the signal source. The receiver was also a small shear wave sensor mounted at the plate edge as in the previous experiment shown at the top of Figure 7. The unreflected signal transmitted through a small distance ($\sim$1 in.) was detected by the edge-mounted receiver and recorded. Using the same transmitter source and receiver, the signal with many reflections present was then detected at a distance of 30 in. from the source. These two signals are shown in Figures 9a and 9b.

The unreflected pulse was also recorded on an X-Y recorder at the output of a sampling oscilloscope. This X-Y recording permitted accurate determination of amplitudes incrementally along the pulse. The pulse was then added to itself in

amplitude with phase shift information determined for the different ray paths reflected within the plate. These reflection factors and phase shifts were available using an EDPM program called "Snell Detail" previously set up at BNW. Attenuation differences for different ray paths were found to be small, since the attenuation was only about 1.3 dB/ft at the frequency used (about 1.6 MHz).

In Table 2, the total time delays (in μsec) of the first 20 reflected ray paths are given in Column 7. In addition, Columns 1-6 give the ray path reflection n-1, the reflection angle θ, the phase delay per reflection $\Delta\phi$ (from "Snell Detail"), the total reflection phase delay $(n-1)\,\Delta\phi$, the total reflection phase delay in μsec $\frac{(n-1)\Delta\phi P}{360^\circ}$, and the time difference Δt, in μsec due to geometric differences in ray paths. The frequency f and the period P for the pulse are also given. The total delays were then used to displace in time each of the first 20 reflected ray paths. The θ values of all rays were such that the reflected ray amplitudes were within less than 0.1% of being totally reflected as calculated by "Snell Detail." The resulting synthesized signal is shown in Figure 9c, and its similarity to the measured signal at 30 in. is apparent.

Several other items are worthy of discussion. The shear wave receiver used in the measurements was about 0.15 in. across its face. From Equation (19) in the previous section, the value of n is 47 for the 1/2-in. A-212-B plate thickness, when the distance is 30 in. from the source, and the frequency is 1.6 MHz. These values make the calculated number of reflections, n-1, equal to 46. Inclusions of the additional reflections in Figure 9c would add further structure in the signal beyond about 16 μs. However, the addition of these many reflections by hand calculation appeared too time consuming, and only the first 20 were added. Also, hand calculations are easily subject to errors which may be accumulative. It appears

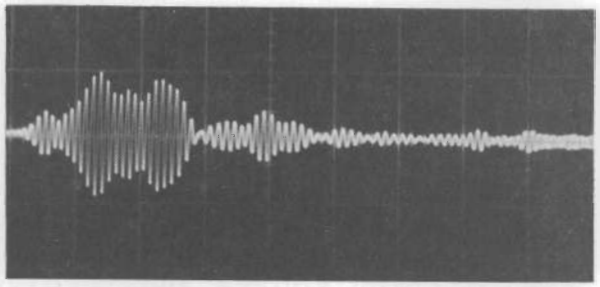

a) Source near same side of Plate edge as Receiver

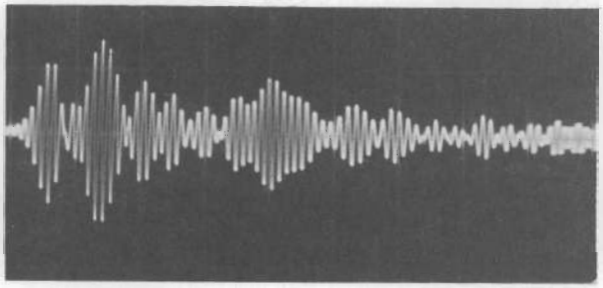

b) Source at Center and Receiver at one side of Plate Edge

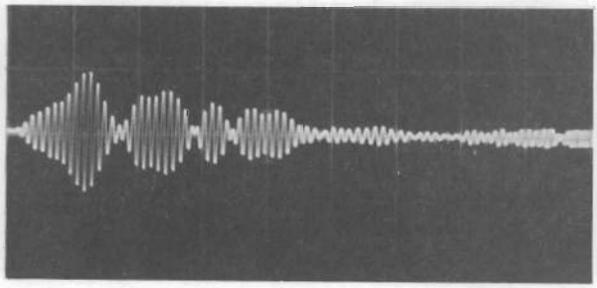

c) Source and Receiver Located near Opposite Surfaces of Plate edge

FIGURE 10. Signals as Received from Various Source Elevations

that pulse synthesis could best be done in future studies electronically with laboratory equipment or with EDPM calculations.

It should be noted that, in adding subsequent ray path signals, all of the first 20 were inadvertently used. Inspection of Figure 1a shows that the original assumptions permitted location of the source at either surface, but not both. Therefore, if the edge-mounted transmitting source and receiver had been located near the same surface of the plate, only the odd ray path reflections should have been used. With source and receiver located near opposite surfaces, only the even reflections should have been used. However, all reflections representing the unlikely occurrence of identical sources at both surfaces were used in the calculations.

The situation in Figure 1b, although including all reflections, is only approximately represented by the equations derived earlier. Since corrections in the hand calculations would be excessively time consuming, transmitting sources were used at both surfaces and the receiver was located at one surface. While this arrangement used in obtaining the measured signal (Figure 9b) is considered impractical, it effectively represents the possibilities of the signal pulse synthesis method.

Following completion of the previously described experiments, photographs of other signals were taken with the transmitting source located at only one elevation position. The source was located first at the same side as the receiver, then at the center of the plate, and then at the side opposite the receiver, as shown in Figure 10a, 10b, and 10c, respectively. This experiment illustrates an effect important to practical test applications. Substantial differences in the three signals prove the feasibility of determining not only the range of an acoustic emission source but also its distance below

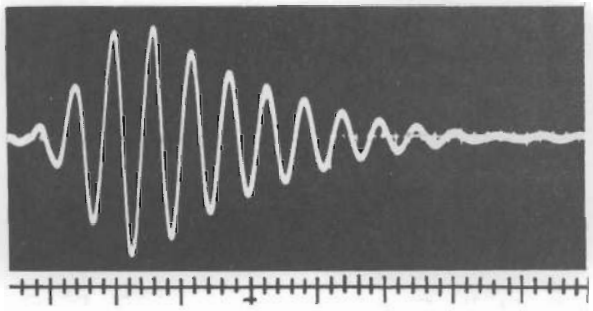

1μS

a) Measured Signal About 1 inch

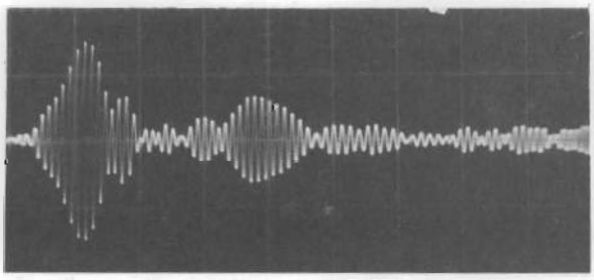

5μS

b) Measured Signal at 30 Inches

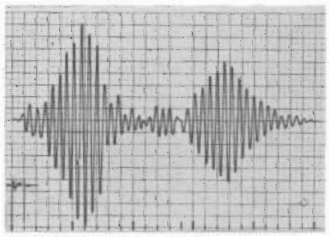

5μS

c) Calculated Signal at 30 Inches

FIGURE 9. Measured Constructed Ultrasonic Signals

TABLE 2. Total Time Delays

Ray Path Reflections, n-1	θ, °	Δφ, °	(n-1)Δφ, °	Δφ/360° (P)(μs)	Δt, μs	Total Delay, μs
Direct Ray from Top	90	0	0	0	0	0
Direct Ray from Bottom	89.05	173.6	173.6	0.298	0.0325	0.330
1	88.1	167.4	167.4	0.287	0.13	0.417
2	87.15	161	322	0.552	0.293	0.845
3	86.2	154.7	464	0.796	0.52	1.32
4	85.2	148.2	594	1.02	0.812	1.83
5	84.3	142.4	712	1.22	1.11	2.33
6	83.35	136.4	819	1.40	1.51	2.91
7	82.4	130.5	914	1.565	2.0	3.57
8	81.5	125	1000	1.71	2.49	4.20
9	80.5	119	1071	1.84	3.23	5.07
10	79.6	113.7	1137	1.95	3.7	5.65
11	78.7	108.5	1193	2.045	4.4	6.45
12	77.8	103.5	1242	2.13	5.2	7.33
13	76.85	98.2	1277	2.19	6.05	8.24
14	75.9	93.2	1305	2.24	7	9.24
15	75.05	88.8	1331	2.285	8	10.29
16	74.2	84.52	1350	2.315	9	11.32
17	73.35	80.34	1365	2.34	10	12.34
18	72.45	76.03	1370	2.35	11.2	13.55
19	71.55	71.83	1365	2.34	12.7	15.04
20	70.7	67.98	1360	2.33	13.6	15.93

f = 1.62 MHz

P = 0.617 μs

$\frac{(n-1)\Delta\phi P}{360°}$

the surface. In making possible the practical use of this capability, it will probably be necessary to generalize the ray reflection studies and perform more elaborate calculations and demonstration experiments.

CONCLUSIONS AND RECOMMENDATIONS

The studies reported herein indicate that acoustic emission test problems for a variety of situations encountered in practice can eventually be simulated in the laboratory. Prior to actual field applications, test parameters should be investigated and optimized. The pulse synthesis analysis should be mathematically generalized and made easier to use through EDPM calculations or suitable laboratory electronic equipment. The methods should also be extended to curved shells and pipes.

ACKNOWLEDGMENTS

The discussions with, and suggestions of, P. H. Hutton regarding these studies are greatly appreciated. The numerous contributions by members of the Nondestructive Testing Methods Development Section Staff who supplied transducers, test samples, etc., are also acknowledged.

DISTRIBUTION

No. of Copies

OFFSITE

1 AEC Chicago Patent Group
G. H. Lee

4 AEC Division of Reactor Development and Technology
E. H. Davidson, Engr & Test
R. R. Newton, RDT (3)

228 AEC Division of Technical Information Extension

1 Atomic Energy of Canada, Ltd.
M. M. Gupta

1 Commonwealth Edison Company
E. C. Bailey

1 Phillips Petroleum Co., NRTS
Idaho Falls, Idaho 83401
D. L. Parry

ONSITE-HANFORD

1 AEC Chicago Patent Group
R. K. Sharp (Richland)

3 AEC RDT Site Representative
P. G. Holsted (2)
J. B. Kitchen

1 AEC Richland Operations Office
C. L. Robinson

3 Battelle Memorial Institute

1 Douglas United Nuclear, Inc.
DUN File

No. of Copies

37 Battelle Northwest

C. A. Bennett
R. L. Brown, Jr.
S. H. Bush
R. G. Chafin
J. H. Cox
K. O. Creek
G. J. Dau
J. W. Helm
D. O. Hunter
P. H. Hutton (10)
W. D. Jolly
R. L. Knecht
V. I. Neeley
R. N. Ord
H. N. Pedersen
R. L. Richardson
C. B. Shaw
J. C. Spanner
J. C. Tobin
D. C. Worlton
FFTF Library - D. D. Taylor
Technical Information (5)
Technical Publications (2)